Electronic Supplementary Material (ESI) for Sustainable Energy & Fuels.

Supporting Information

Modifying the 316L Stainless Steel Surface by Electrodeposition Technique: Towards High-Performance Electrodes for Alkaline Water Electrolysis

Ahmed Zaki Alhakemy [a,b,c], Abu Bakr Ahmed Amine Nassr [d], Abd El-Hady Kashyout [d], Zhenhai Wen [a,b*]

[a] *CAS Key Laboratory of Design and Assembly of Functional Nanostructures, and Fujian Key Laboratory of Nanomaterials, Fujian Institute of Research on the Structure of Matter, Chinese Academy of Sciences, Fuzhou, Fujian 350002, China*

[b] *University of Chinese Academy of Sciences, Beijing 100049, China.*

[c] *Chemistry Department, Faculty of Science, Al-Azhar University, Assiut 71542, Egypt.*

[d] *Electronic Materials Research Department, Advanced Technology and New Materials Research Institute (ATNMRI), City of Scientific Research and Technological Applications (SRTA-City), New Borg Al-Arab City, Alexandria 21934, Egypt*

***Corresponding author**

E-mail: wen@fjirsm.ac.cn (Zhenhai Wen)

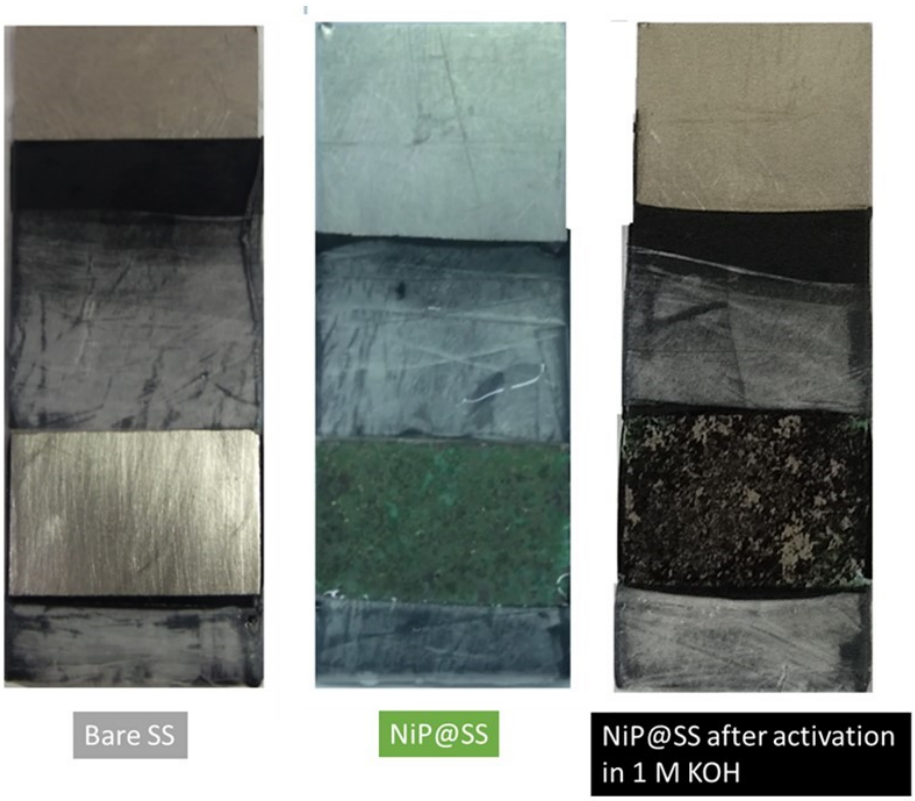

Fig. S1. Photos of SS: left before NiP electrodeposition, middle after *x*NiP electrodeposition, and right after activation of *x*NiP in 1.0M KOH.

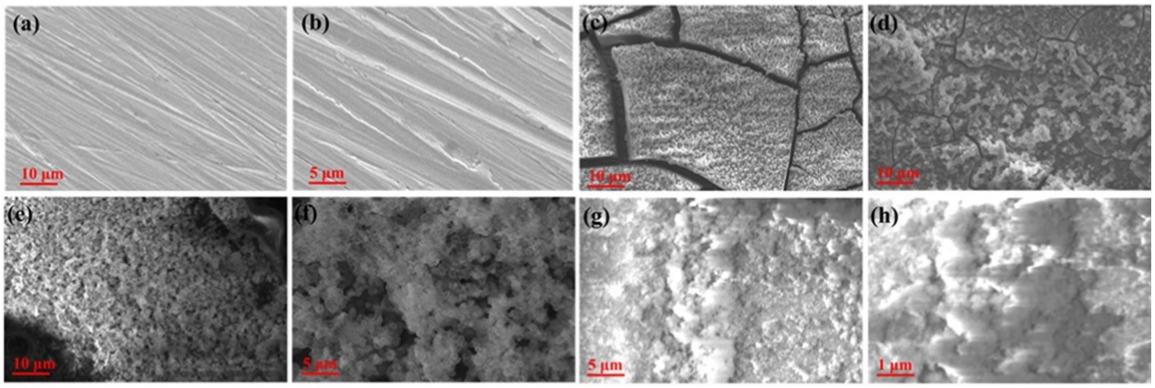

Fig. S2. SEM images of bare SS (a and b); *x*NiP@SS electrodes at different deposition times c) 5 min, d) 10 min, and e-f) 15 min; g-h) SEM images of Ni@SS electrode at 15 min.

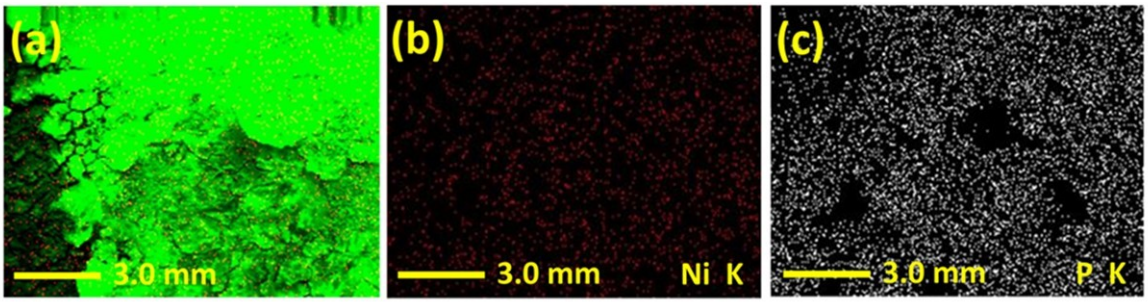

Fig. S3. SEM-EDX elemental mapping of 15NiP@SS electrode.

Table S1: Elemental analysis of *x*NiP@SS nanoparticles determined by EDX analysis

Catalyst	**Averaged atomic % (EDS)**	
	Ni	P
@ Shortest deposition time (5NiP@SS)	51.94	48.06
@ Longest deposition time (20NiP@SS)	52.745	47.255

Video S1. The deposition process of *x*NiP on SS surface at -20 mA cm^{-2}.

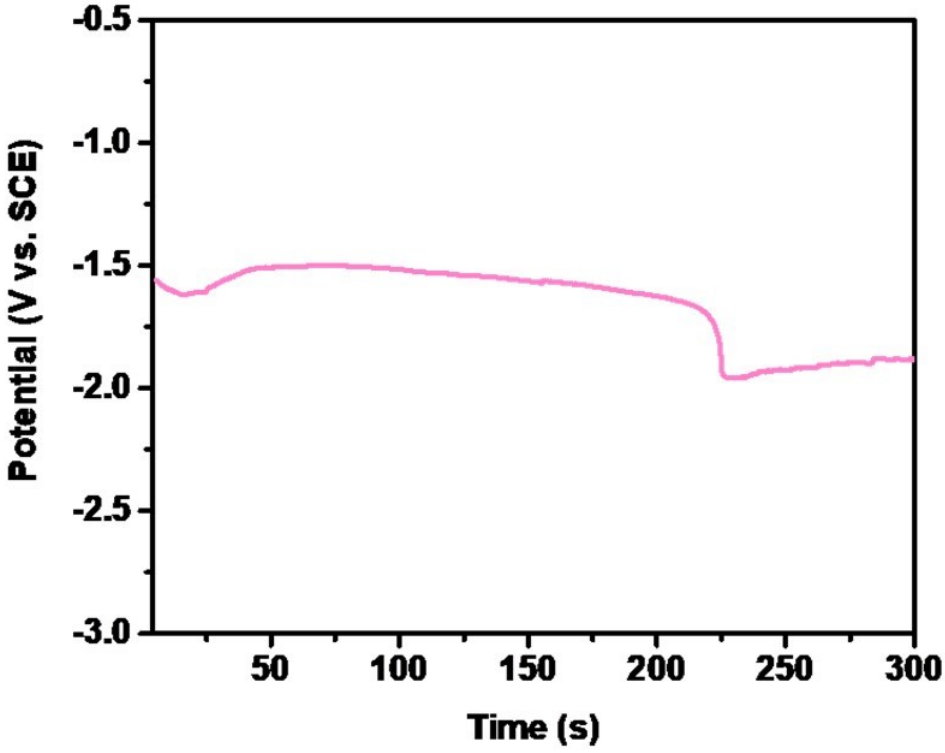

Fig. S4. The time-potential curve for the deposition process.

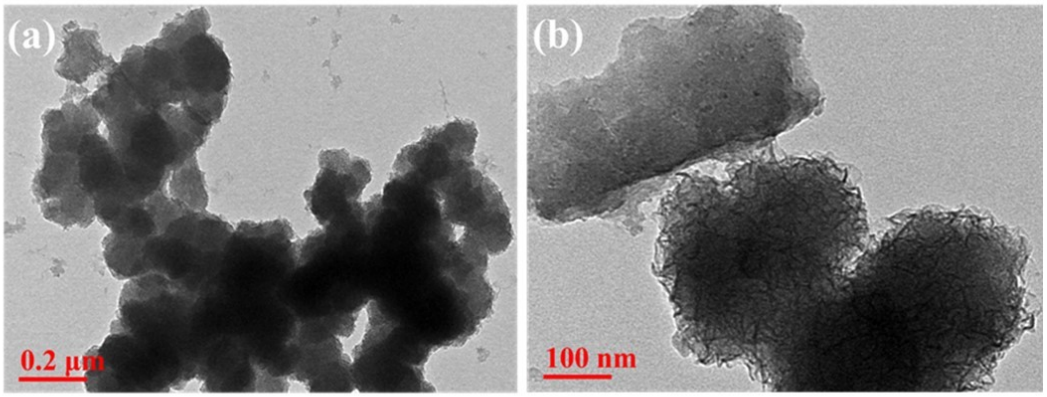

Fig. S5. (a) Low-magnification and (b) high-magnification TEM images of 15NiP@SS.

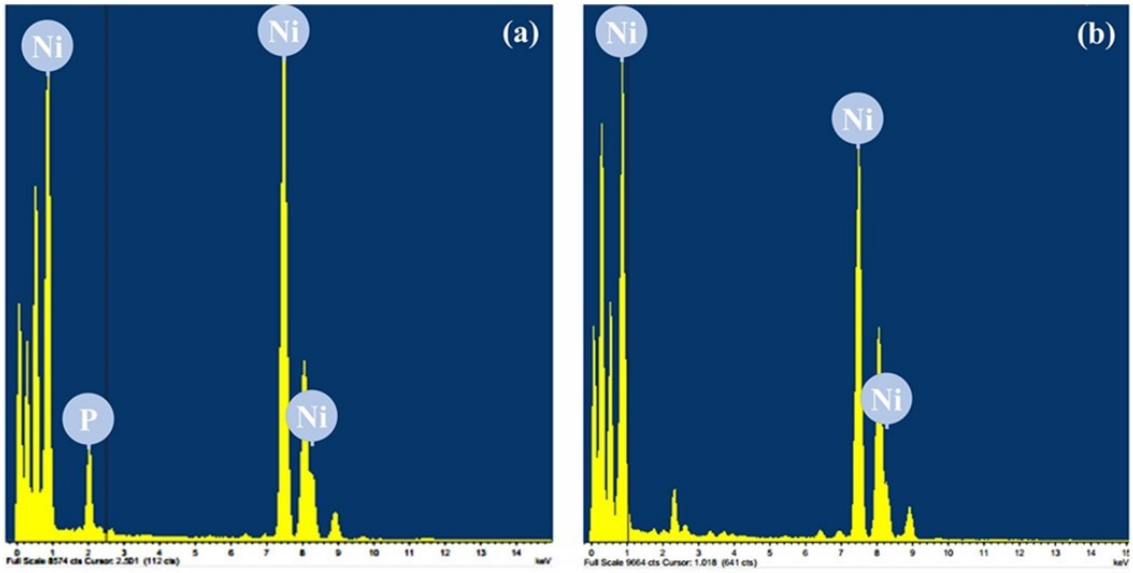

Fig.S6. The TEM-EDX images of 15NiP@SS (a) and Ni@SS (b).

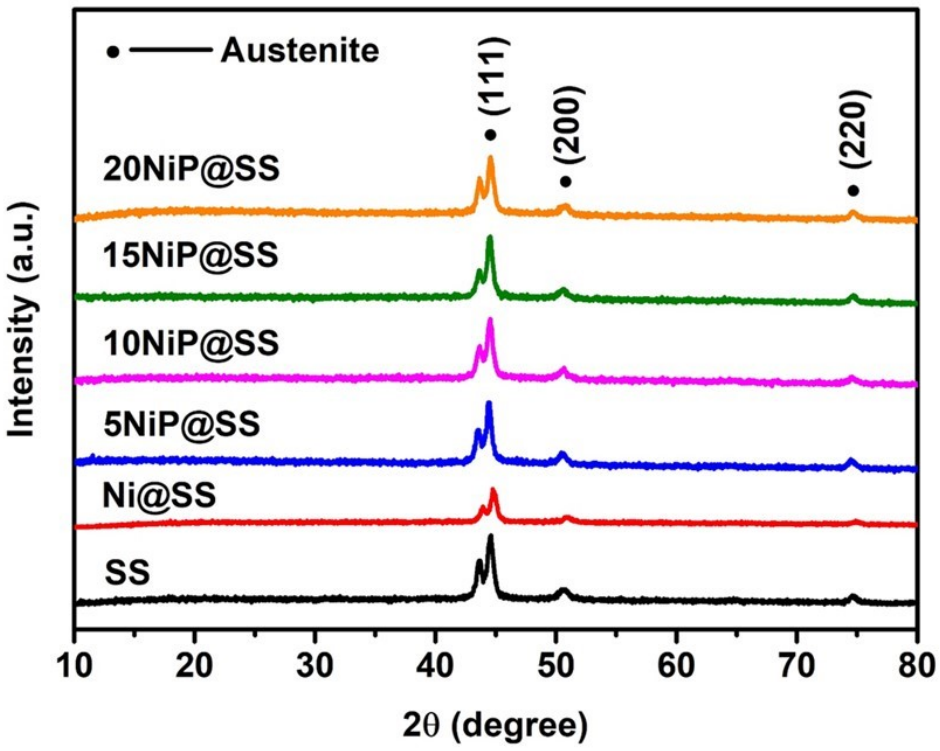

Fig. S7. XRD pattern of bare SS, Ni@SS, 5NiP@SS, 10NiP@SS, 15NiP@SS, and 20NiP@SS samples.

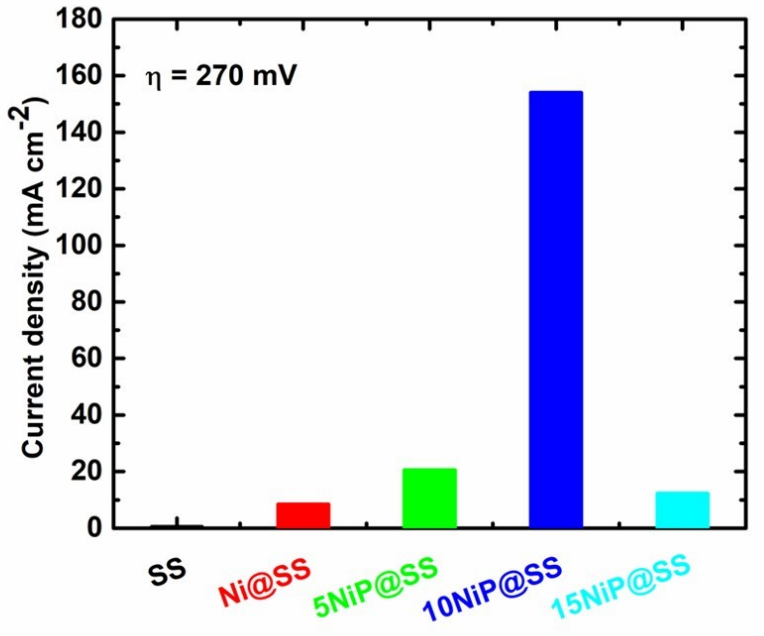

Fig. S8. Current densities of OER for all prepared catalysts at an overpotential of 270 mV

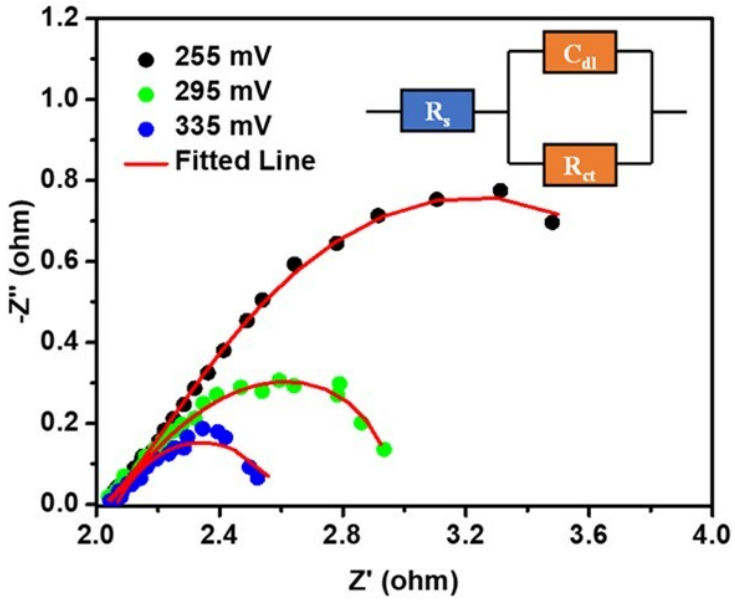

Fig. S9. Nyquist plots of 10NiP@SS recorded at increasing the overpotentials of OER over frequency range of 100 kHz to 100 mHz in 1 M KOH.

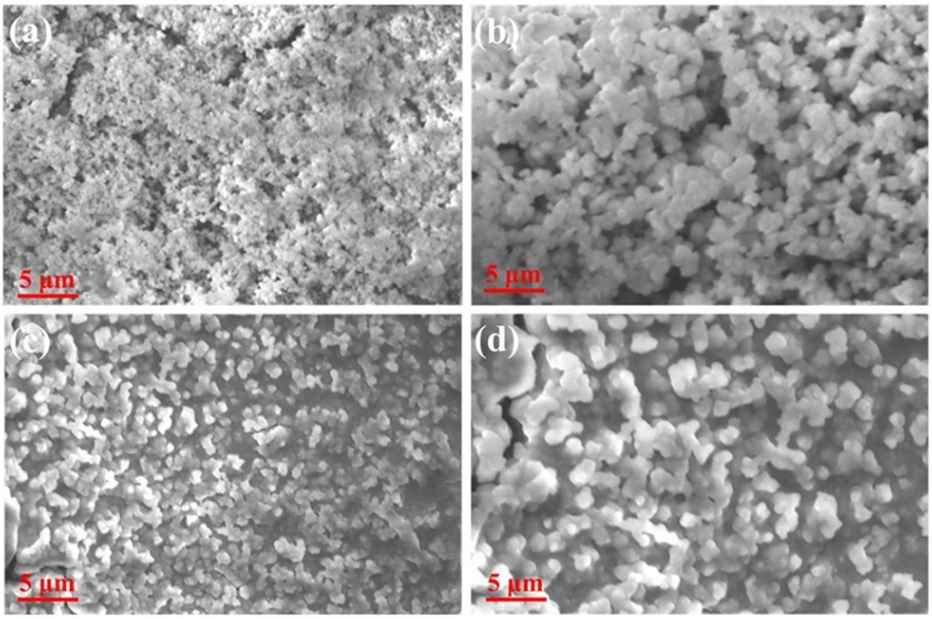

Fig. S10. SEM images of 10NiP@SS (a and b) after activation in 1 M KOH solution and (c and d) after OER stability for 24h

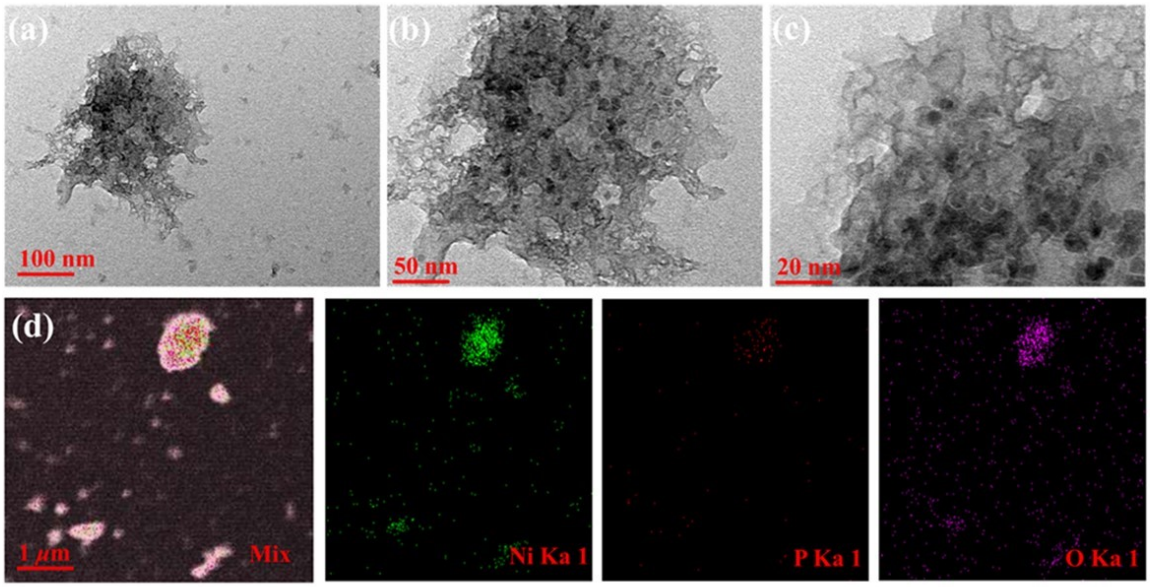

Fig. S 11. TEM images (a-c) and elemental mapping (d) of 10NiP@SS after KOH activation.

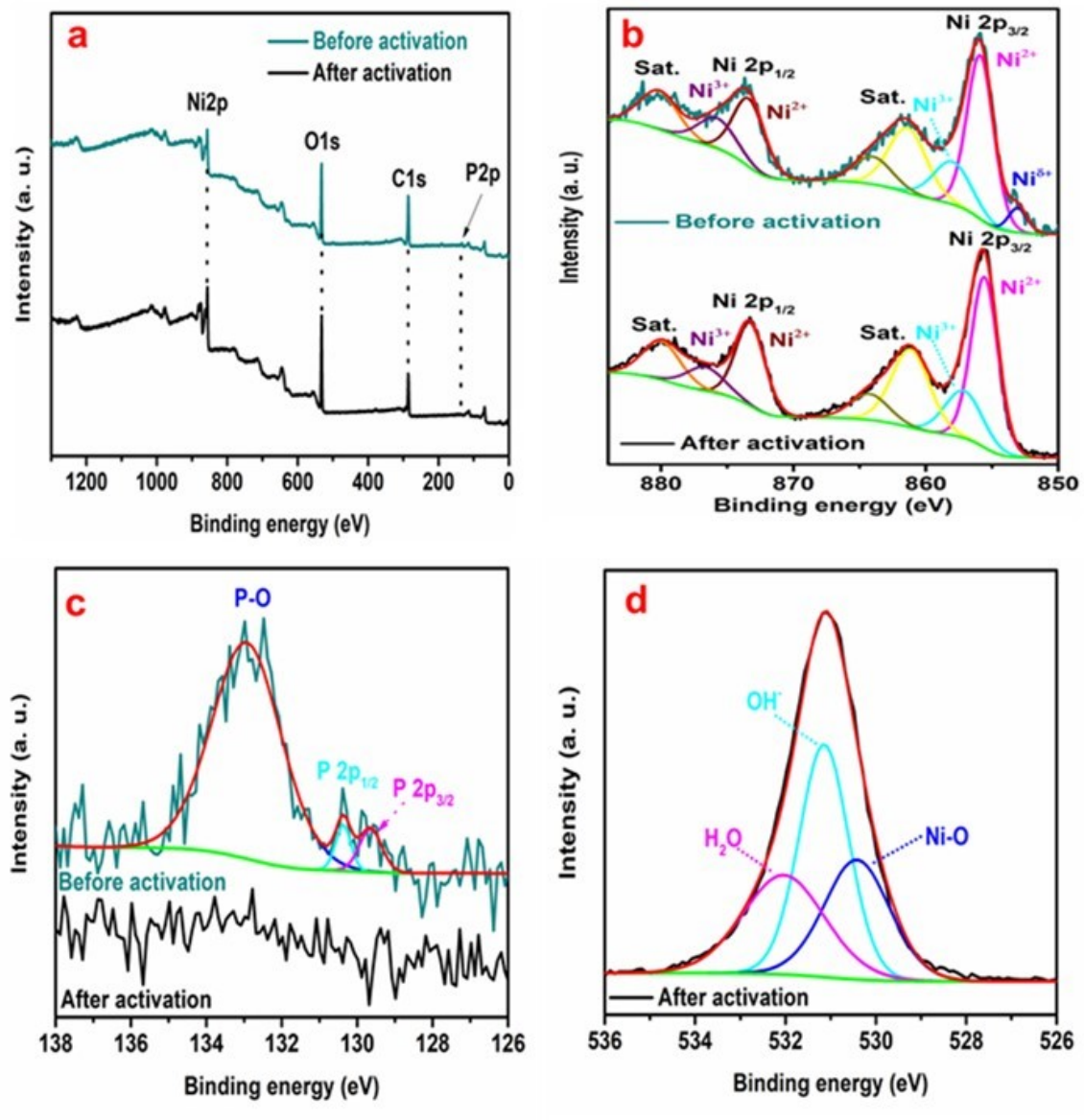

Fig. S12. XPS analysis of 10NiP@SS before and after activation: (a) XPS survey spectrum, (b) Ni 2p region, and (c) P 2p region.

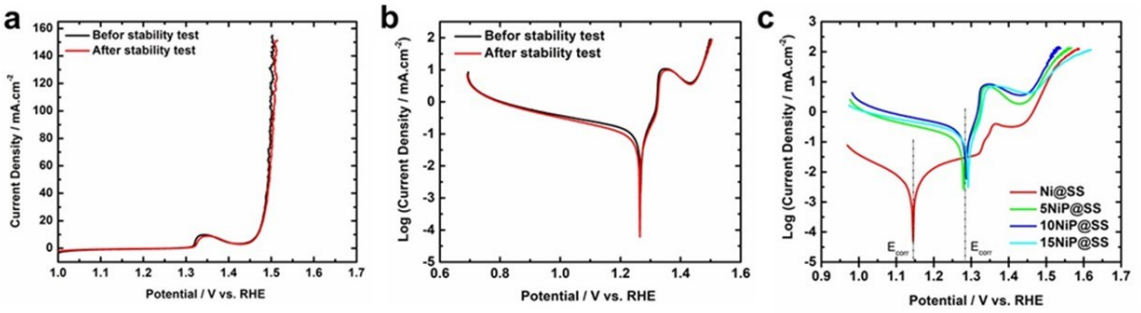

Fig. S13. a) LSV curves and b) Corrosion behavior for 10NiP@SS in 1M KOH solution before and after Chronopotentiometry stability test for 24h. c) Corrosion behavior for the as-prepared *x*NiP@SS electrods and Ni@SS in 1M KOH.

Table S2. Comparison of the 10NiP@SS catalyst with recently published Ni phosphide- and SS-based catalysts for the OER in alkaline electrolytes.

Catalysts	Method of modification	Electrolyte	Overpotential (mv) at specific current density	Tafel plot (mV dec^{-1})	Ref.
10NiP@SS	**Electrodeposition at room temperature**	**1 M KOH**	**238@10 271@100**	**41.42**	**This work**
Ni@SS	**Electrodeposition at room temperature**	**1 M KOH**	**274@10 338@100**	**42.82**	
Bare SS	**-**	**1 M KOH**	**321@10 427@100**	**71.02**	
N, O-codoped nickel phosphide (NO/NiP@CP)	Hydrothermal process followed by pyrolysis under air and N_2 atmospheres	1 M KOH	364@10	108.9	[1]
Hierarchical Ni–Co–P hollow nanobricks (HNBs)	Template-engaged strategy followed by sequential etching and phosphorization treatments	1 M KOH	270@10	76	[2]
Ni_2P/NF	Two-step hydrothermal-phosphorization process	1 M KOH	290@50 320@100	110	[3]
Fe, Mo- codoped Ni_3P	Electrodeposition	1 M KOH	250@0 290@100	-	[4]
Co_3O_4@Ni_2P-CoP/NF	Phosphating and carbonating Co_3O_4 nanowires template-directed fabrication Ni-substituted ZIF-67 arrays onto a 3D Ni foam substrate.	1 M KOH	298@50	75	[5]
Mo-Ni_3S_2/Ni_xP_y	Solvothermal followed by phosphorization	1 M KOH	238@50	60.6	[6]
Mo-NiCoP	Hydrothermal followed by phosphorization	1 M KOH	269@10 364@100	76.7	[7]
Highly porous Ni-P	Electrodeposition	1 M KOH	279@10	39.5	[8]
OESSC	Acid etching followed by oxidizing by heating	1 M KOH	290@10	38.0	[9]

	and CH_4 plasma treatment, respectively.				
Sulfurized stainless steel foil (SSFS)	Annealing process in presence of sulfur at 500 °C under Ar atmosphere.	1 M KOH	262@10	42.0	[10]
316 L SS ex situ-activated	Anodic dissolution of the 316 L metals followed by their possible precipitation in the 5 M LiOH electrolyte.	1 M KOH	300@10 330@100	42	[11]
N-doped surface-etched stainless-steel mesh (NESS)	Exfoliation method followed by annealing process at 400 °C	1 M KOH	278@10	83.0	[12]
Elox_SS	Thermal sulfurization in H_2S/Ar atmosphere at 500 °C followed by electrooxidation process in KOH	1 M KOH	267@10	77.1	[13]
Se-SS	Thermo-selenization followed by acid etching process.	1 M KOH	264@100	36	[14]
SSM-Ni-P (SSM= stainless steel mesh)	Chemical bath deposition of Ni followed by phosphorization under thermal decomposition	1 M KOH	223@10	43.0	[15]
N-doped anodized stainless-steel mesh (NASSM)	Anodic oxidation (4 °C, 10V) followed by nitrogenization (450 °C, NH_3)	1 M KOH	225@10	49.7	[16]
434 SS scrubber	Direct use	1 M KOH	418@10	63	[17]
Stainless-steel fiber felt (SSFF)	Electrochemical induction with cyclic voltammetry (CV) in KOH solution	1 M KOH	230@10 279@100	44.0	[18]
CNT/SS	Atmospheric pressure chemical vapor deposition (APCVD) method	1 M KOH	297@10	66.7	[19]
OxCNT/SS	APCVD method followed by oxidation process in conc. H_2SO_4 and conc. H_2SO_4 solution containing		267@10	44.0	

	$KMnO_4$ and $NaNO_3$ at 40 °C				
$RuO_2/O_xCNT/SS$	APCVD method followed by oxidation process (in conc. H_2SO_4 and conc. H_2SO_4 solution containing $KMnO_4$ and $NaNO_3$ at 40 °C) and a hydrothermal process.		217@10	38.8	
Modified Ni42 steel	Anodization process	0.1 M KOH	254@10	71.6	[20]
		1 M KOH	215@10	-	
Modified AISI 316 steel	Hydrothermal combined in situ electrochemical oxidation–reduction cycle (EORC) method	1 M KOH	280@10	34	[21]
$Ni_{0.33}Co_{0.67}S_2$ NN/SS	Two-step hydrothermal method		286@50	55	[22]
FeNi LDH@NWSSF	Non-woven stainless steel fabrics (NWSSF) were fabricated by wet lay-up papermaking process and followed by a heat treatment process and FeNi LDH@NWSSF was synthesized through a urea-assisted hydrothermal method on NWSSF.	1 M KOH	210@10	56	[23]
Modified AISI 304-12 h	Hydrothermal corrosion process in the presence of an equimolar mixture of KOH and NaOCl at 180 °C for 12 h.	1 M KOH	260@10	41.0	[24]
Fe(Ni)OOH modified SS	Oxidation process by immersing SS in an alkaline oxidant solution containing NaOH and $(NH_4)_2S_2O_8$ for 12 h	1 M KOH	300@10	34	[25]
NiS@SLS	Hydrothermal method	0.1 MKOH	297@11	47.0	[26]
Oxidized Steel	Oxidation process by	0.1 M	347@2	-	[27]

S235	chlorine gas	KOH			
$Ni(Fe)O_xH_y$/SS	Hydrothermal method at 100 °C	1 M KOH	230@20	36	[28]
$Ni(OH)_2$/316L stainless steel nanoparticles on Ni foam	Electrophoretic deposition (EPD) based co-deposition method	1 M KOH	220@10	42	[29]
Elox300-AISI 304	Anodization process at a current density of 1.77 A cm^{-2} in 7.2 M NaOH	1 M KOH	212@12	-	[30]
		0.1 M KOH	269@10	49	

Table S3. Comparison of overpotential at 10, 50 and 100 mA cm^{-2} and R_{ct}. for bare SS, Ni@SS, 5NiP@SS, 10NiP@SS,15NiP@SS, 20NiP@SS and Pt-C@SS in case of HER.

Electrode	**Overpotential**		
	η_{10}	**η_{50}**	**η_{100}**
Bare SS	**428**	**544**	**--**
Ni@SS	**376**	**496**	**--**
5NiP@SS	**288**	**378**	**--**
10NiP@SS	**285**	**366**	**423**
15NiP@SS	**268**	**348**	**403**
20NiP@SS	**277.5**	**366**	**424**
Pt/C@SS	**84**	**231**	**374**

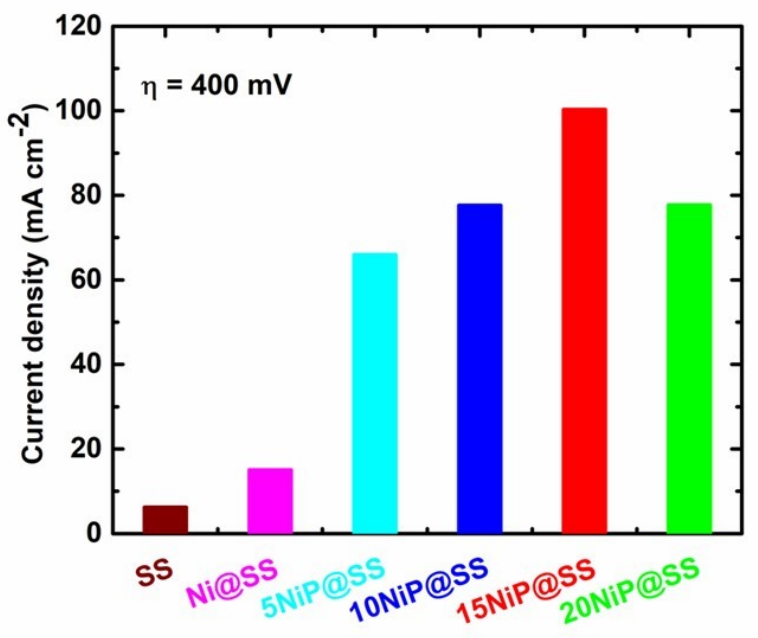

Fig. S14. Current densities for all prepared catalysts at an overpotential of 400 mV for HER.

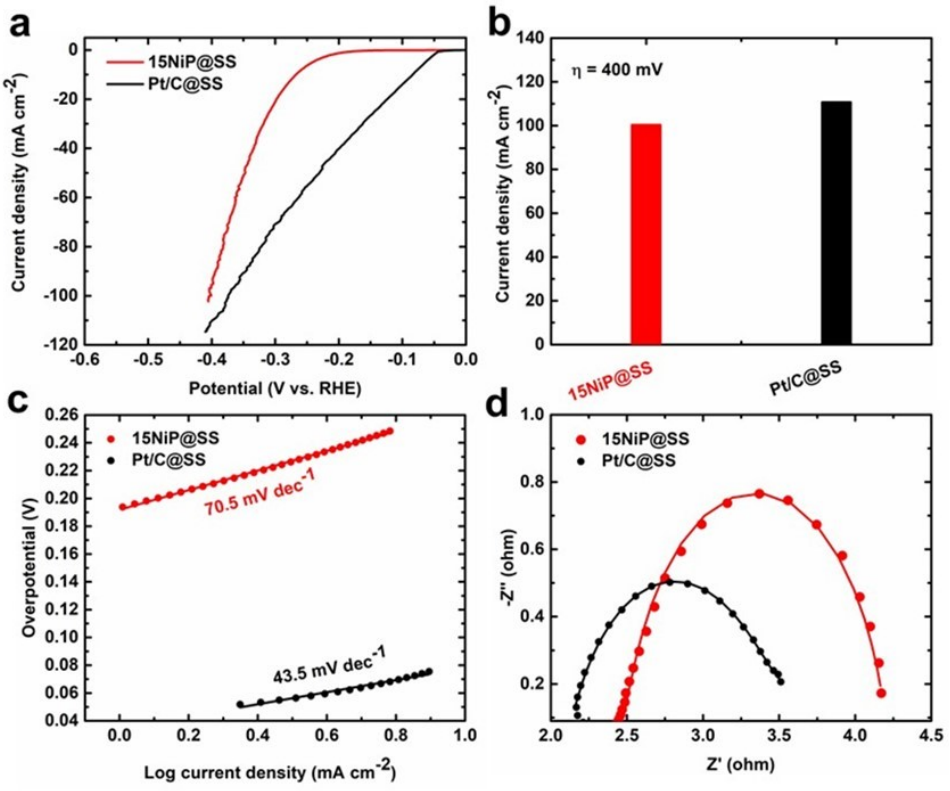

Fig. S15. HER electrocatalytic performance of Pt-C@SS and 15NiP@SS. a) LSV Polarization curves at 1 mV/s scan; b) Current densities at an overpotential of 400 mV; c) Tafel plots; d) Nyquist plots at -1.3 V vs. Hg/HgO.

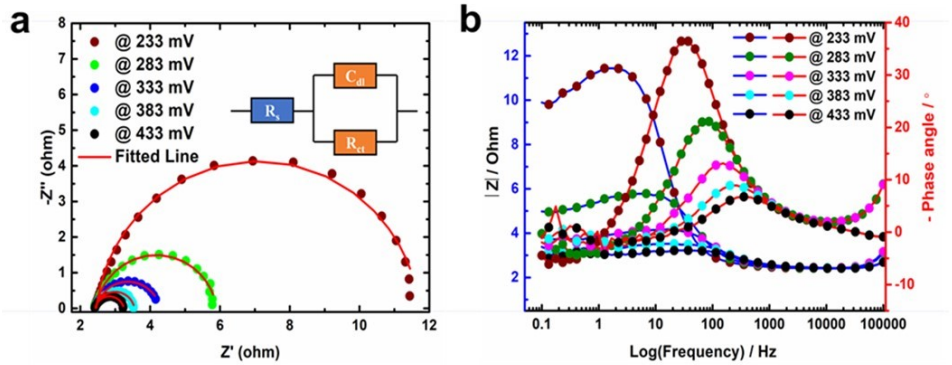

Fig. S16. a) Nyquist plots and b) Bode plots of 15NiP@SS electrode recorded at increasing overpotentials for HER.

Table S4: EIS data of HER on SS, Ni@SS and *x*NiP@SS electrodes .

Catalyst	R_s (Ohm)	R_{ct} (Ohm)	C_{dl} (F)	ECSA (cm^2)	Roughness factor (σ)
SS	2.29	23.06	2.07 x 10^{-04}	10.3	06.89
Ni@SS	2.16	10.32	2.27 x 10^{-04}	11.4	07.58
5NiP@SS	2.63	03.05	5.84 x 10^{-04}	29.2	19.50
10NiP@SS	2.17	02.36	5.93 x 10^{-04}	29.7	19.80
15NiP@SS	2.44	01.84	7.27 x 10^{-04}	36.4	24.20
20NiP@SS	2.19	02.39	5.99 x 10^{-04}	30.0	20.00

Table S5: EIS data of HER on *15*NiP@SS electrode at different potentials.

@ Overpotential (vs. HER)	R_s (Ω)	R_{ct} (Ω)	C_{dl} (F)	ECSA (cm^2)	Roughness factor (σ)
233 mV	2.45	9.26	11.00 x 10^{-04}	55.1	36.7
283 mV	2.44	3.46	08.61 x 10^{-04}	43.0	28.7
333 mV	2.44	1.84	07.27 x 10^{-04}	36.4	24.2
383 mV	2.43	1.12	05.97 x 10^{-04}	29.9	19.9
433 mV	2.42	0.82	05.48 x 10^{-04}	27.4	18.3

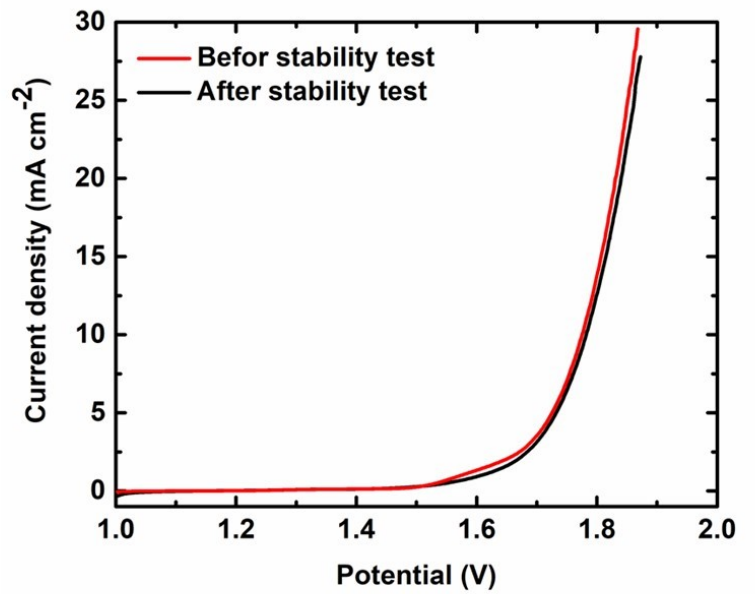

Fig. 17. Polarization curves of 15NiP@SS // 10NiP@SS couple before and after stability tests.

Table S6. Comparison of the 15NiP@SS catalyst with recently published Ni phosphide- and SS-based catalysts for the HER in alkaline electrolytes.

Catalysts	Method of modification	Electrolyte	Overpotential (mv) at specific current density	Tafel plot (mV dec^{-1})	Ref.
15NiP@SS	**Electrodeposition at room temperature**	**1 M KOH**	**268 @10**	**70.5**	**This work**
Ni@SS	**Electrodeposition at room temperature**	**1 M KOH**	**376@10**	**109.63**	
Bare SS	**-**	**1 M KOH**	**428@10**	**117.93**	
Ni_2P/CNS	Pyrolysis process followed by hydrothermal process	0.1 M KOH	315@10	120	31
$Ni_2P/Ni_{12}P_5$	Hydrothermal method at 140 °C	1 M KOH	234@10	98	32
$Ni_{12}P_5$			248@10	100	
Ni_2P			258@10	169	
Ni_3P	Pyrolysis process at 700 °C for 24 h	1 M NaOH	291@10	119	33
Ni_2P nanoparticles	Thermal reaction of NaH_2PO_2 and $NiCl_2 \cdot 6H_2O$ at 250 °C	1 M KOH	250@10	100	34
Ni_2P film	Deposition of nickel layer using a Semicore electron-beam evaporator followed by phosphorization process	1 M KOH	200@10	-	35
NiFeP			255@10		
FeP			300@10		
NiFe LDH-NS@ defective graphene	Exfoliation followed by electrostatic flocculation	1 M KOH	300@10	-	36
EG/$Co_{0.85}Se$/NiFe-LDH	Two hydrothermal process	1 M KOH	~265@10	160	37
$CoNi_2S_4$	Hydrothermal method	1 M KOH	280@10	85	38
Modified Ni42 steel	Anodization process	1 M KOH	299@10	117.5	20
SS scrubber	Direct use	1 M KOH	373@10	121	17
$Ni_{0.33}Co_{0.67}S_2$ NN/SS	Two-step hydrothermal method	1 M KOH	350@30	76	22
N, P doped SS316L	Exfoliation method followed by annealing	1 M KOH	230@10		12

	process at 400 °C				
Etched SS304 (ESS)	Immersing process in 1 M HCl solution at 60 °C for 1.5 h.	1 M KOH	466 @10	-	39
Pristine anodized SS304 (EASS)	Etching process in HCl followed by anodization process		370 @10	-	
Activated anodized SS304 (EASS-Ar/H_2)	Etching process in HCl followed by anodization process and thermal annealing process in Ar/H_2 at 650 °C for 1 h		244 @10	-	
CNT/SS	Atmospheric pressure chemical vapor deposition (APCVD) method	1 M KOH	334@10	119.6	19
OxCNT/SS	APCVD method followed by oxidation process in conc. H_2SO_4 and conc. H_2SO_4 solution containing $KMnO_4$ and $NaNO_3$ at 40 °C		257@10	105.6	

Table S7. Comparison of the overall water splitting performance for the 10NiP@SS (+) || 15NiP@SS (-) catalyst with recently published Ni phosphide- and SS-based catalysts in alkaline electrolytes.

Catalysts	Method of modification	Electrolyte	Overpotential (mv) at 10 mA cm^{-2}	Ref.
***10*NiP@SS (+) || 15NiP@SS (-)**	**Electrodeposition at room temperature**	**1 M KOH**	**1.77**	**This work**
NiS/Ni_2P (+) || NiS/Ni_2P (-)	Hydrothermal followed by sulfurization and phosphorization	1 M KOH	1.67	[40]
$C@Ni_8P_3$ (+) || $C@Ni_8P_3$ (-)	solvothermal procedure	1 M KOH	1.65	[41]
Ni_8P_3 (+) || Ni_8P_3 (-)			1.79	
Ni_5P_4@ Ni foil (+) || Ni_5P_4@ Ni foil (-)	Heating of nickel foil and red phosphorus for 1 h at 550 °C under an inert atmosphere	1 M KOH	1.7@10	[42]
$Ni_2P/Ni(PO_3)_2$ (+) || $Ni_2P/Ni(PO_3)_2$ (-)	Hydrolysis process followed by pyrolysis and phosphorization	1 M KOH	1.63	[43]
Ni–P/CF (+) || Ni–P/CF (-)	Electrodeposition	1 M KOH	1.68	[44]
Ni_2P/NF (+) || Ni_2P/NF (-)	Thermal reaction of NaH_2PO_2 and $NiCl_2 \cdot 6H_2O$ at 250 °C	1 M KOH	1.63	[45]
NESS (+) || NESSP (-)	Exfoliation method followed by annealing process at 400 °C	1 M KOH	1.74	[12]
SS scrubber (+, -)	Direct use	1 M KOH	1.98	[17]
CNT/SS (+, -)	Atmospheric pressure chemical vapor deposition (APCVD) method	1 M KOH	1.95	[19]
OxCNT/SS (+, -)	APCVD method followed by oxidation process in conc. H_2SO_4 and conc. H_2SO_4 solution containing		1.83	
NASSM (+, -)	Anodic oxidation (4 °C, 10V) followed by nitrogenization (450 °C, NH_3)	1 M KOH	1.61	[16]
$Ni_{0.33}Co_{0.67}S_2$ NN/SS	Two-step hydrothermal method	1 M KOH	1.67	[22]
FeNi LDH@NWSSF	Non-woven stainless steel fabrics (NWSSF) were fabricated by wet lay-up papermaking process and	1 M KOH	1.56	[23]

	followed by a heat treatment process and FeNi LDH@NWSSF was synthesized through a urea-assisted hydrothermal method on NWSSF.			

Video S2: Hydrogen and oxygen production during the full water splitting test at 10 mA cm^{-2}.

Video S3: Hydrogen and oxygen production during the full water splitting test at 20 mA cm^{-2}.

Video S4: Hydrogen and oxygen production during the full water splitting test at 50 mA cm^{-2}.

References

1. P. Bhanja, Y. Kim, B. Paul, Y. V. Kaneti, A. A. Alothman, A. Bhaumik and Y. Yamauchi, *Chem. Eng. J.*, 2021, **405**, 126803.
2. E. Hu, Y. Feng, J. Nai, D. Zhao, Y. Hu and X. W. Lou, *Energy Environ. Sci.*, 2018, **11**, 872-880.
3. Y. Li, X. Jiang, Z. Miao, J. Tang, Q. Zheng, F. Xie and D. Lin, *ChemCatChem*, 2020, **12**, 917-925.
4. S. M. Pawar, A. T. Aqueel Ahmed, C. H. Lee, P. T. Babar, J. H. Kim, S. U. Lee, H. Kim and H. Im, *ACS Appl. Energy Mater.*, 2021, **4**, 14169-14179.
5. M. Guo, Y. Li, L. Zhou, Q. Zheng, W. Jie, F. Xie, C. Xu and D. Lin, *Electrochim. Acta*, 2019, **298**, 525-532.
6. X. Luo, P. Ji, P. Wang, R. Cheng, D. Chen, C. Lin, J. Zhang, J. He, Z. Shi, N. Li, S. Xiao and S. Mu, *Adv. Energy Mater.*, 2020, **10**, 1903891.

7. J. Lin, Y. Yan, C. Li, X. Si, H. Wang, J. Qi, J. Cao, Z. Zhong, W. Fei and J. Feng, *Nano-Micro Lett.*, 2019, **11**, 55.

8. D. Song, D. Hong, Y. Kwon, H. Kim, J. Shin, H. M. Lee and E. Cho, *J. Mater. Chem. A*, 2020, **8**, 12069-12079.

9. Y. Lyu, R. Wang, L. Tao, Y. Zou, H. Zhou, T. Liu, Y. Zhou, J. Huo, S. P. Jiang, J. Zheng and S. Wang, *Appl. Catal. B: Environ.*, 2019, **248**, 277-285.

10. X. Liu, B. You and Y. Sun, *ACS Sustainable Chem. Eng*, 2017, **5**, 4778-4784.

11. F. Moureaux, P. Stevens, G. Toussaint and M. Chatenet, *Appl. Catal. B: Environ.*, 2019, **258**, 117963.

12. M.-S. Balogun, W. Qiu, Y. Huang, H. Yang, R. Xu, W. Zhao, G.-R. Li, H. Ji and Y. Tong, *Adv. Mater.*, 2017, **29**, 1702095.

13. M. Lee, M. S. Jee, S. Y. Lee, M. K. Cho, J.-P. Ahn, H.-S. Oh, W. Kim, Y. J. Hwang and B. K. Min, *ACS Appl. Mater. Inter*, 2018, **10**, 24499-24507.

14. Y. Xiao, T. Hu, X. Zhao, F. X. Hu, H. B. Yang and C. M. Li, *Nano Energy*, 2020, **75**, 104949.

15. Y. Gao, T. Xiong, Y. Li, Y. Huang, Y. Li and M. S. J. T. Balogun, *ACS Omega*, 2019, **4**, 16130-16138.

16. M. Yao, B. Sun, N. Wang, W. Hu and S. Komarneni, *Appl. Surf. Sci.*, 2019, **480**, 655-664.

17. S. Anantharaj, S. Chatterjee, K. C. Swaathini, T. S. Amarnath, E. Subhashini, D. K. Pattanayak and S. Kundu, *ACS Sustainable Chem. Eng*, 2018, **6**, 2498-2509.

18. S. Zhu, C. Chang, Y. Sun, G. Duan, Y. Chen, J. Pan, Y. Tang and P. Wan, *Int. J. Hydrog. Energy*, 2020, **45**, 1810-1821.

19. H. Zhang, J. M. de Souza e Silva, X. Lu, C. S. de Oliveira, B. Cui, X. Li, C. Lin, S. L. Schweizer, A. W. Maijenburg, M. Bron and R. B. Wehrspohn, *Adv. Mater. Inter.*, 2019, **6**, 1900774.

20. H. Schäfer, D. M. Chevrier, P. Zhang, J. Stangl, K. Müller-Buschbaum, J. D. Hardege, K. Kuepper, J. Wollschläger, U. Krupp, S. Dühnen, M. Steinhart, L. Walder, S. Sadaf and M. Schmidt, *Adv.Funct. Mater.*, 2016, **26**, 6402-6417.

21. H. Zhong, J. Wang, F. Meng and X. Zhang, *Angew. Chem.*, 2016, **128**, 10091-10095.

22. G. He, W. Zhang, Y. Deng, C. Zhong, W. Hu and X. Han, *Catalysts*, 2017, **7**, 366.

23. L. Wang, X. Huang, S. Jiang, M. Li, K. Zhang, Y. Yan, H. Zhang and J. M. Xue, *ACS Appl. Mater. Inter*, 2017, **9**, 40281-40289.

24. S. Anantharaj, M. Venkatesh, A. S. Salunke, T. V. S. V. Simha, V. Prabu and S. Kundu, *ACS Sustainable Chem. Eng*, 2017, **5**, 10072-10083.

25. D. Tang, O. Mabayoje, Y. Lai, Y. Liu and C. B. Mullins, *ChemistrySelect*, 2017, **2**, 2230-2234.

26. J. S. Chen, J. Ren, M. Shalom, T. Fellinger and M. Antonietti, *ACS Appl. Mater. Inter*, 2016, **8**, 5509-5516.

27. H. Schäfer, K. Küpper, J. Wollschläger, N. Kashaev, J. Hardege, L. Walder, S. Mohsen Beladi-Mousavi, B. Hartmann-Azanza, M. Steinhart and S. Sadaf, *ChemSusChem*, 2015, **8**, 3099-3110.

28. Q. Zhang, H. Zhong, F. Meng, D. Bao, X. Zhang and X. Wei, *Nano Research*, 2018, **11**, 1294-1300.

29. A. Balram, H. Zhang and S. Santhanagopalan, *Mater. Chem. Front.*, 2017, **1**, 2376-2382.

30. H. Schäfer, S. Sadaf, L. Walder, K. Kuepper, S. Dinklage, J. Wollschläger, L. Schneider, M. Steinhart, J. Hardege and D. Daum, *Energy Environ. Sci.*, 2015, **8**, 2685-2697.

31. Y. Li, P. Cai, S. Ci and Z. Wen, *ChemElectroChem*, 2017, **4**, 340-344.

32. S. Surendran, S. Shanmugapriya, S. Shanmugam, L. Vasylechko and R. Kalai Selvan, *ACS Appl. Energy Mater.*, 2018, **1**, 78-92.

33. A. B. Laursen, R. B. Wexler, M. J. Whitaker, E. J. Izett, K. U. D. Calvinho, S. Hwang, R. Rucker, H. Wang, J. Li, E. Garfunkel, M. Greenblatt, A. M. Rappe and G. C. Dismukes, *ACS Catal.*, 2018, **8**, 4408-4419.

34. L. Feng, H. Vrubel, M. Bensimon and X. Hu, *Phys. Chem. Chem. Phys.*, 2014, **16**, 5917-5921.

35. C. G. Read, J. F. Callejas, C. F. Holder and R. E. Schaak, *ACS Appl. Mater. Inter*, 2016, **8**, 12798-12803.

36. Y. Jia, L. Zhang, G. Gao, H. Chen, B. Wang, J. Zhou, M. T. Soo, M. Hong, X. Yan, G. Qian, J. Zou, A. Du and X. Yao, *Adv. Mater.*, 2017, **29**, 1700017.

37. Y. Hou, M. R. Lohe, J. Zhang, S. Liu, X. Zhuang and X. Feng, *Energy Environ. Sci.*, 2016, **9**, 478-483.

38. D. Wang, X. Zhang, Z. Du, Z. Mo, Y. Wu, Q. Yang, Y. Zhang and Z. Wu, *Int. J. Hydrog. Energy*, 2017, **42**, 3043-3050.

39. M. Kim, J. Ha, N. Shin, Y.-T. Kim and J. Choi, *Electrochim. Acta*, 2020, **364**, 137315.

40. X. Xiao, D. Huang, Y. Fu, M. Wen, X. Jiang, X. Lv, M. Li, L. Gao, S. Liu, M. Wang, C. Zhao and Y. Shen, *ACS Appl. Mater. Inter*, 2018, **10**, 4689-4696.

41. J. Yu, Q. Li, N. Chen, C.-Y. Xu, L. Zhen, J. Wu and V. P. Dravid, *ACS Appl. Mater. Inter.*, 2016, **8**, 27850-27858.

42. M. Ledendecker, S. Krick Calderón, C. Papp, H.-P. Steinrück, M. Antonietti and M. Shalom, *Angew. Chem., Int. Ed.*, 2015, **54**, 12361-12365.

43. J. Tong, W. Li, L. Bo, Y. Li, T. Li and Q. Zhang, *Electrochim. Acta*, 2019, **320**, 134579.

44. Q. Liu, S. Gu and C. M. Li, *J. Power Sources*, 2015, **299**, 342-346.

45. L.-A. Stern, L. Feng, F. Song and X. Hu, *Energy Environ. Sci.*, 2015, **8**, 2347-2351.